J Mater Sci: Mater Electron (2022) 33:22810–22820

Indium thermal interface material microstructure as a function of thermal history and bonding metallization

Peter McClure[1,*] and Yujia Wang[2]

[1] Universal Instruments' Advanced Process Laboratory, Conklin, NY 13748, USA
[2] Materials Science and Engineering, Cornell University, Ithaca, NY 14850, USA

Received: 15 April 2022
Accepted: 3 September 2022
Published online: 14 September 2022

© The Author(s), under exclusive licence to Springer Science+Business Media, LLC, part of Springer Nature 2022

ABSTRACT

Indium has gained attention as a thermal interface material (TIM), in high-power electronics, due to its high thermal conductivity and mechanical compliance. However, there is minimal understanding of the indium microstructure as it is challenging to analyze due to its softness. Samples with indium are difficult to cross-section; conventional mechanical polishing is considered impractical. Instead, slow and expensive focused ion beam techniques have been required. In this study, a cross-section procedure for components with indium was developed based on mechanical polishing, ultrasonic cleaning, etching, and ion milling. With this technique, indium cross-sections that showed microstructural details could be made and studied for changes across different bond metallizations and thermal histories. Electronic packages with indium TIM bonded to Au or Ag metalized Si chips and Ni-coated Cu lids were examined. Intermetallic compounds between In–Au, In–Ag, and In–Ni were investigated with scanning electron microscopy and energy-dispersive X-ray spectroscopy. The effects of bond metallization, doping, and solder reflow cycles (thermal history) on the indium microstructures were examined.

1 Introduction

With the miniaturization of semiconductor devices, the power density of chips climbs, creating an increased demand for materials that can effectively dissipate heat [1–4]. TIMs reduce contact resistance and conduct heat between two surfaces; while surviving strains from mismatches of the coefficient of thermal expansion of chips and heat spreaders [5–10].

Indium is a promising TIM material due to its high thermal conductivity and ability to deform [1, 11]. To evaluate indium as a TIM analysis of indium in electronic packages under realistic thermal conditions is required.

Cross-sectional analysis of packages with indium is challenging due to indium's soft/ductile nature, leading to smearing and embedded particles. Indium is often reported as too soft to be polished practically

Address correspondence to E-mail: peter.mcclure@uic.com

https://doi.org/10.1007/s10854-022-09048-1

[12–14]. Dasarathy successfully polished and etched pure indium samples and saw grains and twinning [15, 16], but these samples did not have the added complexities of polishing samples with other materials present (like with an electronic package). The use of focused ion beam (FIB) in the cross-section of indium components has been reported [17–20]. Alloys of indium, gold, and nickel have been observed along with cracking along intermetallics with thermal cycling [3]. However, FIB can be expensive, slow, and not compatible with the cross-sectioning of large areas. Interfaces with indium, nickel, and gold have been studied without FIB [21–23] but are limited to examining interfaces and Intermetallic compounds (IMC) that form between indium and other metals. To evaluate indium, as a TIM, it is vital to examine the microstructure of indium in electronic packages. Information on intermetallic growth and bulk microstructure can give insight into a material's long-term reliability. The ability to cross-section large numbers of samples over the entire TIM area would be a key enabler for evaluating indium as a TIM.

Some recent questions about indium as a TIM are how well it bonds to surfaces and how a built package would survive standard solder reflows [24]. Gold and silver layers are often applied to surfaces to aid in bonding to indium, but it is unclear what the indium microstructure is and how these change with subsequent thermal loading. A greater understanding of these factors would allow for better designing systems with indium TIMs, resulting in better thermal performance and product lifetime.

Au or Ag metallizations are added to the Si die and Cu lids to aid bonding to indium. Then flux is added, and a solid indium preform is placed between the die and lid. The system then undergoes a solder reflow cycle that melts the indium and causes bonding with Au or Ag. Because actual products have many components with SAC (tin silver copper) solder, multiple reflows past 240 °C are often needed. Every reflow the indium experiences can change the bonding and microstructure of the system.

In the present work, a cross-section technique for packages with indium was developed; based on mechanical polishing, ultrasonic cleaning, etching (with nitric acid), and ion milling. Ball grid array (BGA) packages with Cu lids (Ag or Au coated), indium solder TIM, and Si chips (Ag or Au coated), processed with different reflow cycles, were inspected by cross-sectioning. The microstructures, interfaces, and defects were examined with a scanning electron microscopy (SEM). The IMCs between In–Au, In–Ag, and In–Ni were studied with energy-dispersive X-ray spectroscopy (EDS). Finally, the role of bond metallization, doping, and heat treatment on indium's microstructure was examined. The cross-section results gave insight into if Ag or Au coating would be sufficient for bonding to indium with multiple SAC reflows.

2 Experimental methods

2.1 Materials

BGA packages with indium TIM were assembled by Indium Corporation®, illustrated in Fig. 1. The BGA packages were 52 × 52 mm, with Si die (15.8 × 19.5 and 1 mm thick), the laminate was 1.8 mm thick, and the copper lids were 3 mm thick with a nickel coating. The metallization on the lids was Au (300–500 nm) or Ag (500–1000 nm); die metallization was Ti (100 nm), Ni (300–500 nm), and Au (300–500 nm) or Ag (500–1000 nm). The lids were held to the laminates by an adhesive on the edges of the lids. Indium preforms (300 µm thick) were used. The indium was bonded by placing flux (proprietary) on the die, placing an indium preform, adding flux to the top of the preform, and placing the Cu lid on top. The constructed assemblies were then processed in a reflow oven. An initial reflow at a peak temperature of 200 °C in 1–2% formic acid vapor/N_2 was done to all the samples to bond the indium. Up to four subsequent SAC reflows, 260 °C peak temperature in air, were done on samples to simulate the BGAs on boards that needed multiple reflows.

Six samples with different metallizations, number of SAC reflows, and doping were examined. Doped indium (with 100 ppm Ge) was used to aid in wetting of indium to gold. Table 1 lists the details of each sample. No repeats of samples were made (samples sizes of 1), and all samples had been stored at room temperature for years before analysis, possibly causing unknown aging effects. Despite these limitations, information on the indium TIM system could be learned, especially considering the minimal work on the subject.

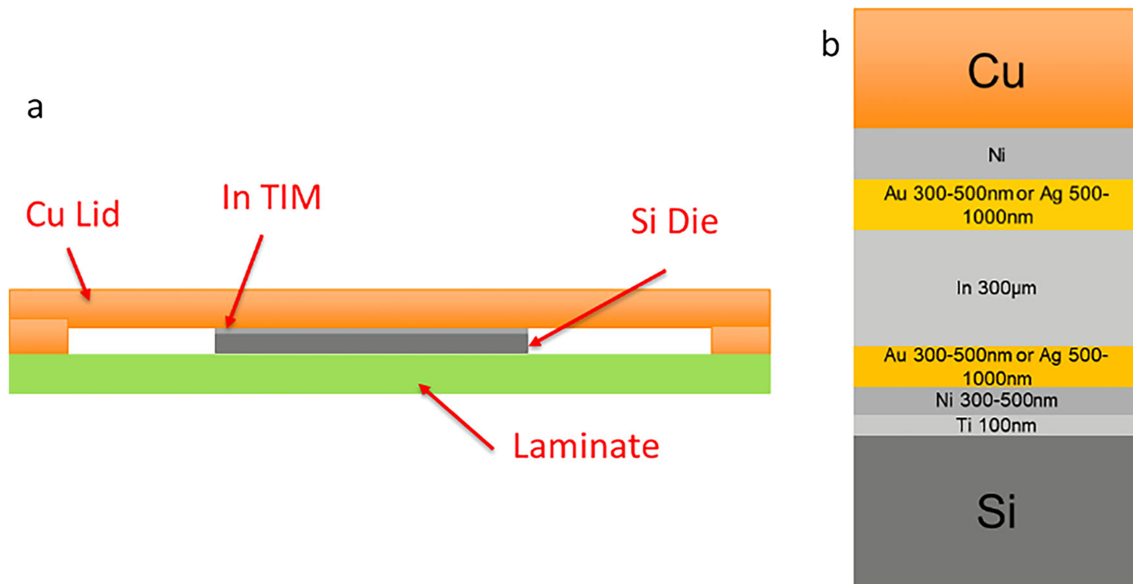

Fig. 1 Generic cross-sectional illustration of samples (**a**) [not to scale] and metallization layers in samples (**b**) [not to scale]

Table 1 Surface finish, SAC reflow cycles, and doping conditions of samples A–F

Sample	Surface finish	SAC reflows	Doping
A	Ag (0.5 μm)	0	N/A
B	Ag (0.5 μm)	4	N/A
C	Ag (1.0 μm)	4	N/A
D	Au (0.3–0.5 μm)	0	N/A
E	Au (0.3–0.5 μm)	0	Ge (100 ppm)
F	Au (0.3–0.5 μm)	3	N/A

2.2 Procedure of cross-sectioning

Due to the soft nature of indium, great care had to be taken to cross-section samples. Polishing with traditional abrasives would always cause some amount of damage to the indium and cause particles to embed in the indium. Chemical etching was used to remove the damaged layer of indium and the embedded particles. Etching could remove indium without adding plastic damage. But etching would unevenly attack different parts of the cross-sections (different materials or topographies). So a procedure of polishing to make a flat section and then etching to remove the damaged indium layer was used. Progressively finer grit could be used, so a thinner damage layer would need to be removed with shorter etching, causing less uneven etching effects. Finally, ion milling was used to remove the remaining damaged indium layer and expose a surface that should not have been damaged by cutting, polishing, or etching.

The procedure used for cross-sectioning the samples is below. Most samples in this report were cross-sectioned with this procedure; some samples had slight variations (polishing time/force, etch time/concentration).

(1) Cut sample to an area of interest with a slow-speed saw and mounted the sections in epoxy (31.5 mm diameter, EpoxySet from Allied High Tech Products. Inc.).
(2) Hand polished: P-800 and P-1200 SiC paper: Until the Ni layer on the lid could be seen.
(3) Etched with 30% HNO3 in water for 50 s: Rinsed thoroughly with water.
(4) Ultrasonically cleaned in isopropanol for 10–25 min, until 80–90% of large Si particles feel out: Checked sample with an optical microscope every 5 min (ultrasonic cleaning could damage samples).
(5) Automated fine polish (RotoPol-22 from Struers Inc.):

- P-4000 SiC paper, 10 N force for 12 min;
- 3 μm suspended diamond: MD-Dac (Polishing cloth from Struers Inc): 15 N for 1.5 min then 10 N for 1.5 min (water flooded during the last 30 s);

- 1 μm suspended diamond, MD-Dac: 15 N for 1.5 min then 10 N for 1.5 min (water flooded during the last 30 s);
- 0.1 μm colloidal alumina, MD-Chem: 15 N for 1.5 min then 10 N for 1 min (water flooded during the last 30 s);
- 0.02 μm colloidal silica, MD-Chem: 10 N for 1 min (water flooded during the last 30 s).

(6) Etched with 30% HNO3 for 20 ~ 30 s: Rinsed thoroughly.

(7) Automated fine polish:

- 0.1 μm colloidal alumina, 10 N for 2.75 min (water flooded during the last 30 s);
- 0.02 μm colloidal silica, 5 N for 1 min, (water flooded during the last 30 s).

(8) Etched with 30% HNO3 for 5 s.

(9) Ion milled surface until microstructure was visible: Samples were sent to Oneida Research Services Inc. (Whitesboro, NY) for milling with a Hitachi IM4000 in flat ion milling mode with Argon for 15–30 min.

2.3 Samples characterization

The cross-sectioned samples were examined with optical microscopy (Leica DMRX) and environmental SEM (FEI XL30) with a backscattered electron (BSE) detector and EDS. The elemental compositions reported from EDS should be considered approximations and not exact values. Electron beam voltage of 25 kV and water vapor pressure was 0.5 torr were used. All images shown are oriented with the lid on the top and the Si die on the bottom.

3 Results and discussion

3.1 Cross-section technique

The developed cross-section procedure involved several techniques that had different effects and limitations. Conventional mechanical polishing could produce a level surface but caused particles embedding in indium, damage to interfaces and indium, and smearing. Etching could remove embedded particles and surface damage, but aggressive etching could destroy Ni and IMC interlayers of interest and make uneven surfaces. Ultrasonic cleaning could partially remove big particles but could not remove small embedded particles (diameters < 20 μm) and would not remove the damaged layer. Ion-milling could remove smeared and damaged layers and some small embedded particles (diameters < 1 μm) but was slow at removing material.

These techniques were combined and sequenced to achieve cross-sectional surfaces with minimal amounts of embedded particles, minimal surface damage, and an analyzable microstructure. The process flow was (1) Get a level surface through mechanical polishing. (2) Remove big embedded particles and the damaged layer with etching and ultrasonic cleaning. (3) Gently polish the surface with finer grit until the Ni interlayer becomes visible. (4) Remove small embedded particles and damage layer by etching. (5) Get level surfaces through finer polishing. (6) Etch to remove excess embedded particles and damage layer. (7) Remove remaining smear/damage and small embedded particles with ion-milling.

The resulting surfaces were sufficient to show microstructures of the indium and its boundaries, Fig. 2, but the surface finish did have limitations. Because the surface preparation did not give a

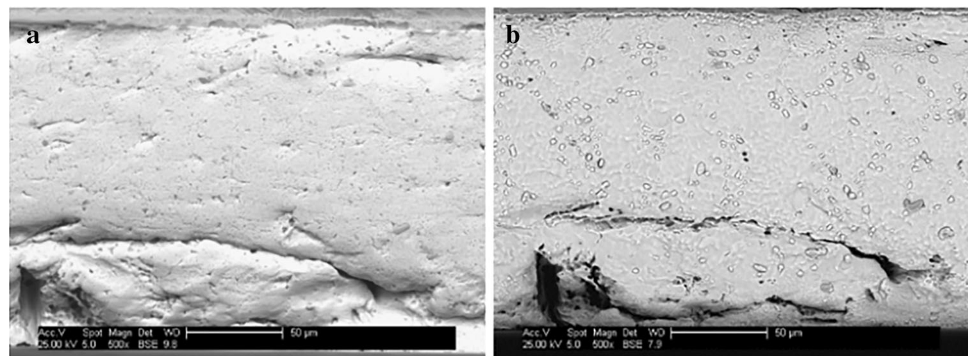

Fig. 2 Surfaces of sample C before (**a**) and after (**b**) ion-milling

smooth/flat surface, techniques such as electron backscatter diffraction, which require smooth/flat surfaces, were inappropriate. During analysis, care also had to be taken to account for possible artifacts from surface topography, unremoved foreign particles, over-etching, or surface preparation.

3.2 Indium bonded to Ag metallization

Figure 3 shows the general microstructural features of bulk indium and interfaces of samples with Ag. For all silver metalized samples, the silver coating on the lids and die had completely diffused into indium and precipitated as silver-rich phases (25–50%Ag, 50–75%In). Most phases contained 25–27% Ag. Along the lid, 3–5 μm thick pure Ni interlayer and a Ni-rich IMC (23% Ni, 77% In) were observed. On the die side, no pure metal interlayer was seen; instead, a Ni-rich IMC layer was observed. In the bulk indium, grain boundary-like features were observed, referred to as grain boundaries in this report. These grain boundaries were similar in shape to those shown in pure indium samples [15, 16]. The Ag-rich particles were found preferentially near the grain boundary features. Grain boundaries could form by the solidification of indium during cooling and could be preferred sites for the precipitation of $AgIn_2$/Ag_2In phases because the sliver phases should have solidified after the bulk indium had crystallized according to the phase diagram [25].

Sample A (0.5 μm Ag, 0 SAC reflows) had some voids in the bulk indium. The voids mainly formed near the center region of the indium, Fig. 4b. Correspondingly to the voids, pump-out (removal of material between the lid and die because of temperature-dependent warpage) of indium was seen. Large volumes of indium extended beyond the die, between the lid and the laminate. The voids and pump-out were likely caused by the warpage of the die and lid during high temperatures, while the indium was liquid (T_m = 157 °C).

A Ni–In rich IMC layer formed continuously along the lid/indium interface, and minimal delamination was seen. However, the IMC layer was discontinuous on the die side. Delamination (1 μm width) occurred in the areas without an IMC layer, Fig. 4a, showing the poor wettability between indium and Si.

Crack-like features were observed in the bulk indium, referred to as cracks in this report. Ag-rich particles were seen with some cracks, Fig. 4a, indicating the cracks propagated along grain boundaries (intergranular cracking). Other cracks did not relate to particles or grain boundaries (transgranular cracking). Cracking was unexpected in indium, a soft metal expected to be mechanically compliant and deform plastically. It is possible that the features were not cracks but a different form of defect.

Sample B (0.5 μm Ag, 4 SAC reflows) had larger voids, more delamination, and more pump-out than sample A (0 SAC reflows), Fig. 5. The large voids could have been caused by the warpage of the die and lid during reflows. The delamination had larger widths (2–5 μm) and primarily occurred at interfaces of IMC/indium (Fig. 5b) and along IMC/Si (Fig. 5a), indicating separation and poor rewetting of IMC/indium and IMC/Si interfaces during SAC reflows. The poor rewetting could be related to oxidation, as the SAC reflow was conducted in air. When melted, air could penetrate and form indium oxides on surfaces, causing poor rewetting. An inert atmosphere during SAC reflows might minimize delamination. Some delamination/cracking seemed to have

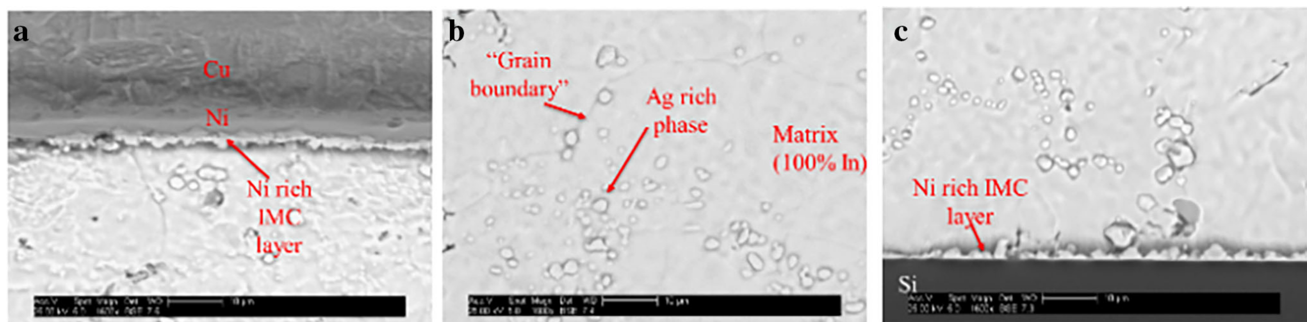

Fig. 3 SEM images of interfaces and bulk indium of Ag samples: sample B (**a**), sample A (**b**, **c**)

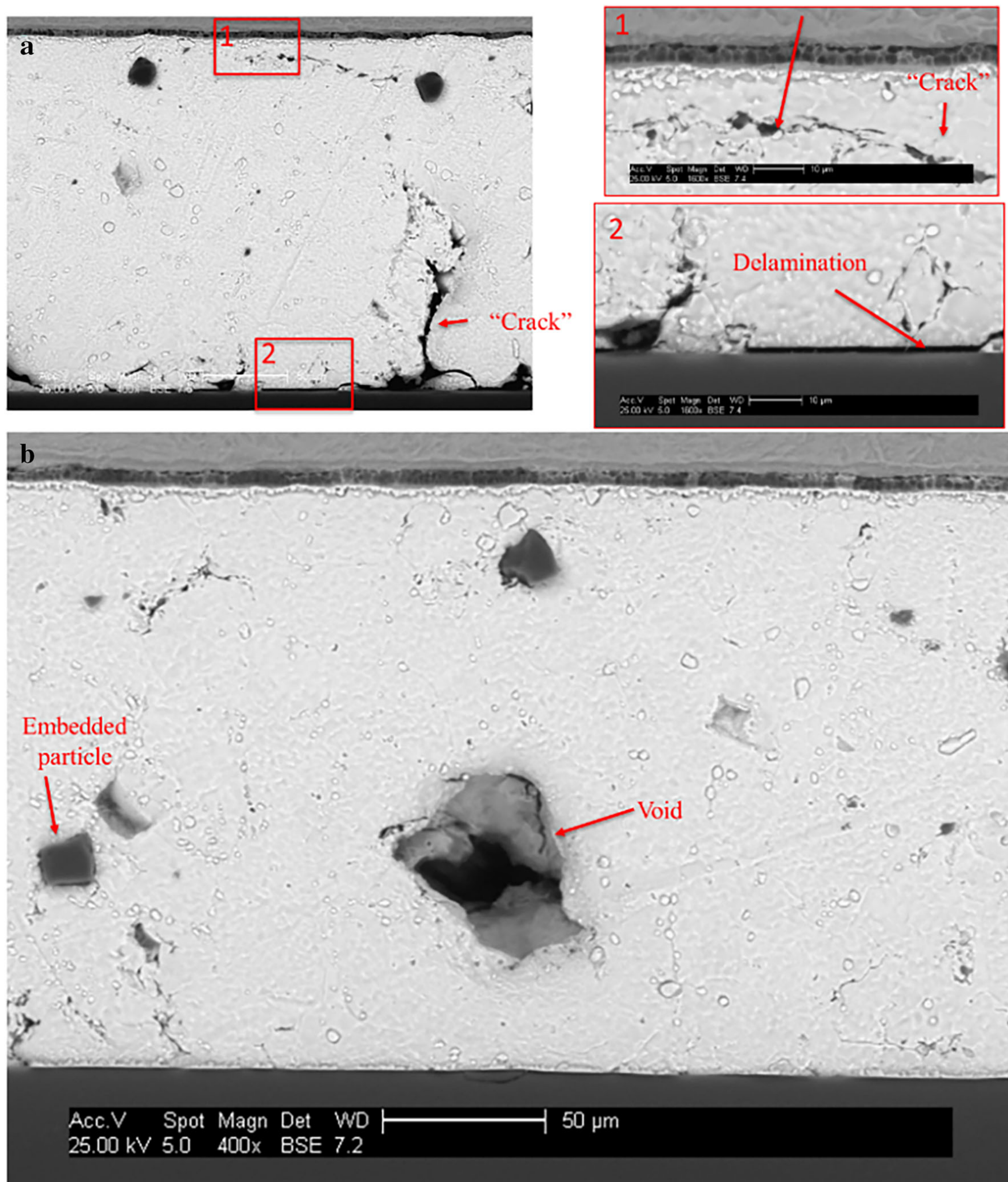

Fig. 4 SEM images of defects in sample A (**a**, **b**)

propagated from the delaminated interfaces of Si/indium, indicating no IMC layer remained, Fig. 5b.

Sample C (1 µm Ag, 4 SAC reflows) had more precipitated Ag-rich particles in bulk indium than sample B with 0.5 µm Ag. The thicker Ag coating was completely depleted after 4 SAC reflows. The remaining Ni layer was discontinuous on the lid side, Fig. 6b. Possibly, the Ni was removed during the added SAC reflows. Correspondingly, some Cu-rich phases (72% Cu, 18% Ag, 10% In) were observed in the bulk indium, showing that Cu had diffused into indium.

Consistent with sample B, this sample had delamination on both sides, large voids, and cracks (Fig. 6), showing the detrimental effect of multiple SAC reflows.

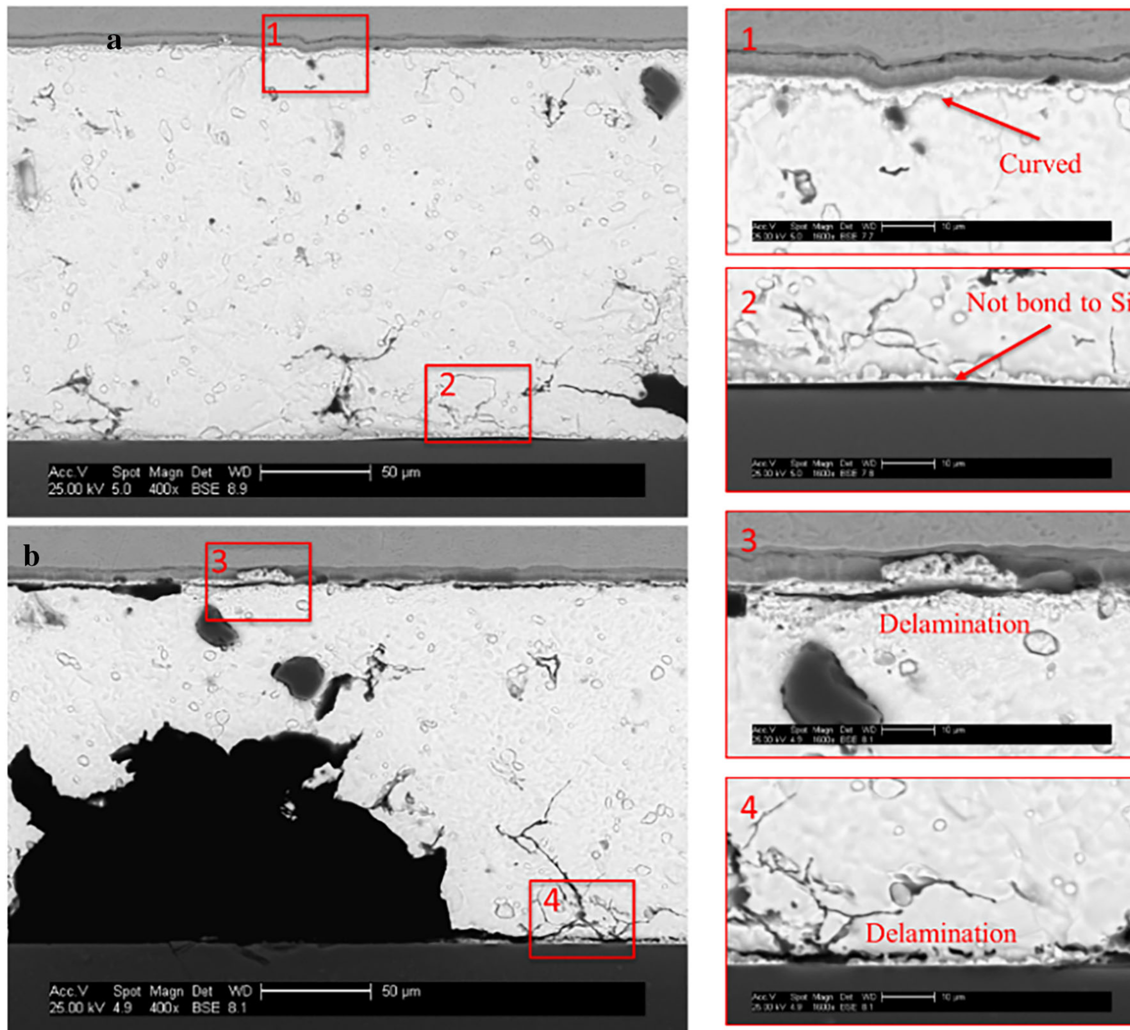

Fig. 5 SEM images of defects in sample B (**a**, **b**)

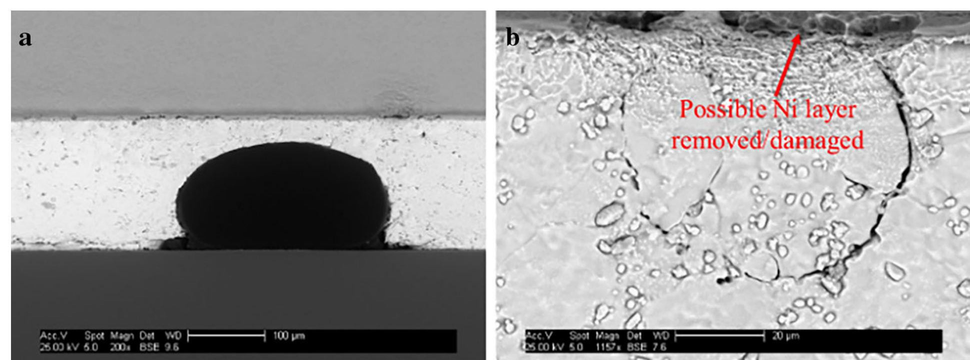

Fig. 6 SEM images of defects in sample C (**a**, **b**)

3.3 Indium bonded to Au metallization

Figure 7 shows the general microstructure of bulk indium and interfaces of samples with Au metallization. Similar to Ag samples, grain boundaries were observed in indium. IMC layers on the lid side were visible but were too thin to be meaningfully analyzed with EDS. Since the IMC layers in Au-coated samples had different morphologies to the Ni-rich IMC in Ag samples, it was inferred that the IMCs

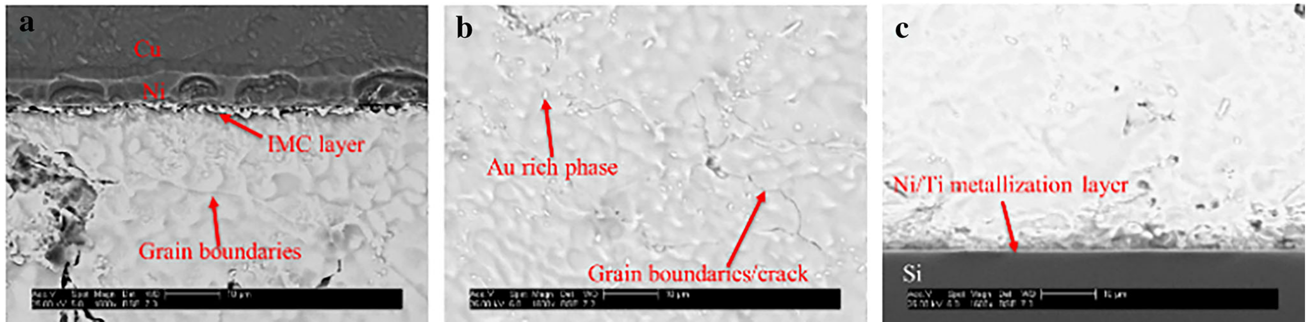

Fig. 7 SEM images of interfaces and bulk indium of sample D (**a**–**c**)

were likely Au–Ni–In rich. Similar Au–Ni–In IMCs in Au-coated indium packages have been reported [2]. On the die side, a thin IMC layer (thickness < 1 μm) was observed, Fig. 7c, implying an Au-rich IMC. The IMC seen on the die side was similar in morphology to the IMC seen on the lid side. Small particles (< 1 μm) were observed in the bulk indium and appeared brighter than indium in the BSE imaging. These particles could be Au-rich phases (33% Au, 67% In) based on the AuIn phase diagram [26].

Sample D (Au, 0 SAC reflows) had larger voids than the Ag sample with 0 SAC reflows. Most of the voids were observed near the interfaces. No delamination was seen. Similar to the Ag samples, transgranular and intergranular cracking was seen.

Sample E (Au, Ge-doped indium, 0 SAC reflows) did not have significant voiding in the bulk indium, Fig. 8. It is possible that the germanium doping mitigated the voiding. Compared to the non-doped Au sample, the Ge-doped sample had more Au-rich phases near the lid side. In addition, a Ni-rich IMC was detected on the lid side, Fig. 9. Indicating that the Au was depleted and that the Ge could have affected the depletion of Au.

Large particles (≥ 5 μm) were observed in bulk indium, Fig. 9b, c. Some of the particles seemed to be attached to the Si surface, Fig. 8b. EDS analysis showed that the big particles were pure indium. Their formation might relate to the doping of Ge, as these features were not seen in any other samples.

On the die side, continuous delamination with a width of 1 μm was formed throughout the sample, Fig. 8a, b. No metallization or Ni–Au rich IMC layer was observed at the delaminated interfaces. It was unclear if Ge doping was related to the delamination.

Small voids (< 1 μm) were seen throughout the bulk indium. The cause for these voids was unclear, but it was not considered likely that the cross-section procedure caused them.

Sample F (Au, 3 SAC reflows) had larger voids and more delamination than sample D (Au, 0 SAC reflows), further showing the detrimental effects of SAC reflows. The delamination mainly occurred between the Ni–Au rich IMC and indium (Fig. 10), indicating the SAC reflows could lead to poor wettability of indium/Ni–Au rich IMC. Similar to sample E, some small voids formed in bulk indium; the cause was unclear.

Unlike Ag samples whose precipitated Ag-rich phases near grain boundaries, the Au sample with 3 SAC reflows had a "network" structure of Au-rich phases, as indicated by the dashed lines in Fig. 11. The particles were arranged in lines that would intersect each other or have other lines that ran parallel, making a "network" structure. Previous work has shown spallation of In–Au IMC [21]. It is possible that SAC reflows caused the IMC to spall and have In–Au particles disperse in the liquid indium. When the indium solidified, the particles could have been trapped in the pattern they had when the indium was liquid.

4 Conclusion

This study developed a cross-section technique for electronic components with indium TIMs. The resulting surface finishes allowed for analysis of indium without significant damage, smearing, or foreign particles. BGAs containing indium TIM with

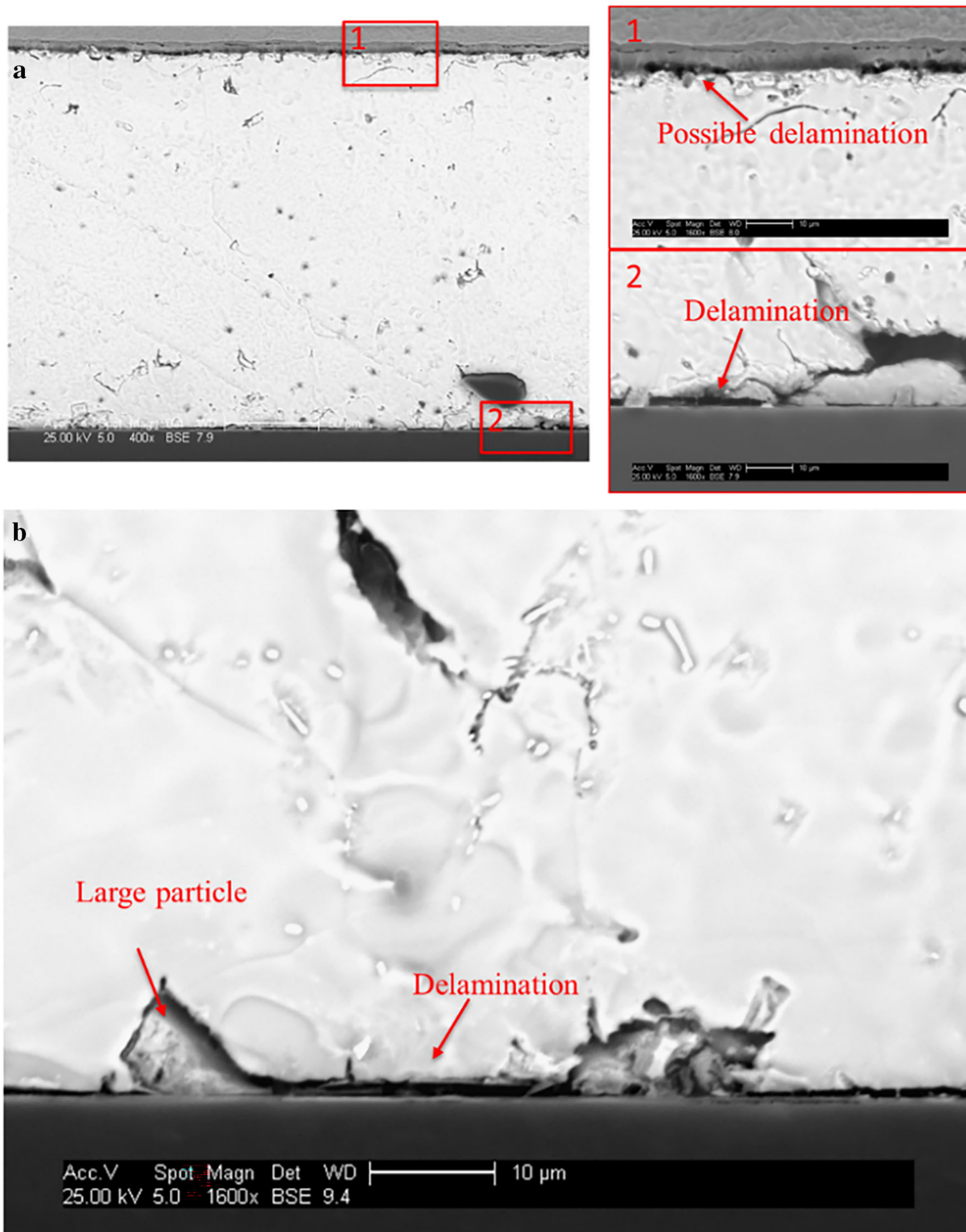

Fig. 8 SEM images of defects in sample E (**a**, **b**)

different bond metallization and thermal histories were examined. Despite sample limitation (sample sizes of one and uneven metallization layers), several findings could be made:

- Ag metallizations fully dissolved into indium and precipitated out Ag-rich phases along grain boundaries.
- Au metallizations formed Ni–Au–In IMCs, but spalling of the IMC likely occurred after SAC reflows.

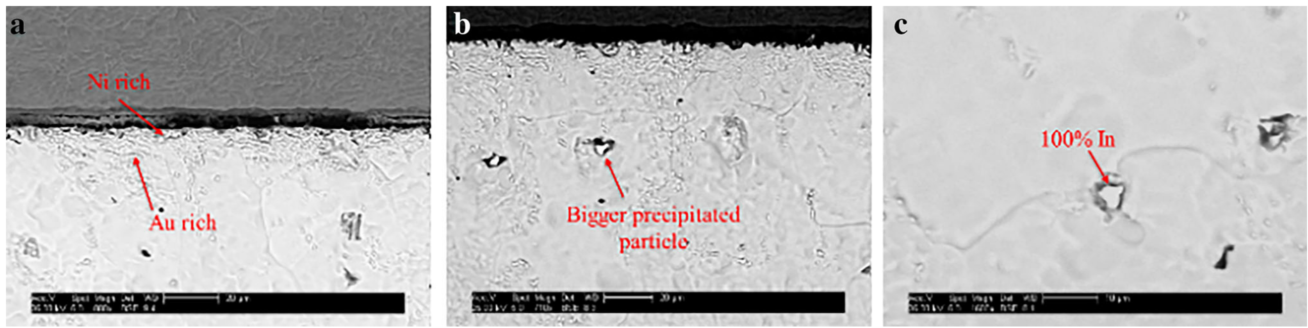

Fig. 9 Variations in sample E (**a**–**c**)

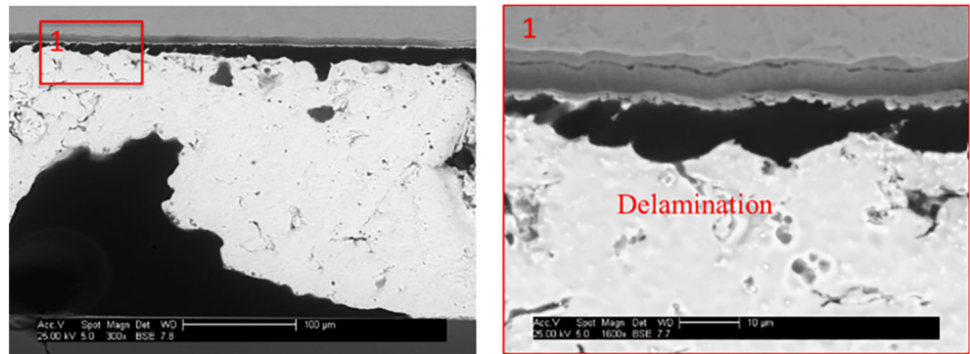

Fig. 10 SEM images of defects in sample F

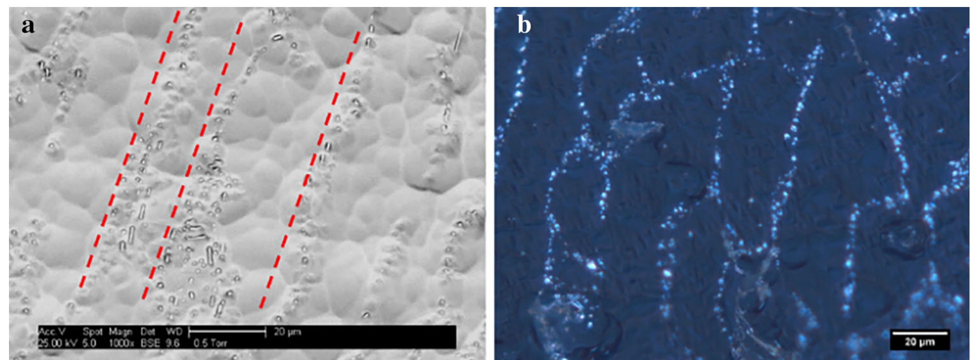

Fig. 11 "Network" structure of Au-rich phases in sample F; SEM (**a**) and polarized light (**b**)

- All samples showed crack-like features in the indium, believed to be both inter-and transgranular cracking.
- SAC reflows added voiding and delamination to both Au and Ag metalized samples.

Acknowledgements

The authors would like to acknowledge Indium Corporation® for providing the BGA samples and the financial support of this study by Universal Instruments' AREA Consortium.

Author contributions

All authors contributed to the study conceptions and design. Sample preparation was done by YW. All authors contributed to the analysis and writing the manuscript. All authors have read and approved the manuscript.

Funding

This work was supported by Universal Instruments' AREA Consortium.

Data availability

The datasets generated during and/or analyzed during the current study are available from the corresponding author on reasonable request.

Declarations

Conflict of interest The authors have no relevant financial or non-financial interests to disclose.

References

1. X. Luo, Y. Zhang, C. Zandén, M. Murugesan, Y. Cao, L. Ye, J. Liu, J. Mater. Sci. **25**, 2333–2338 (2014)
2. J. Hansson, C. Zandén, L. Ye, J. Liu, *IEEE-NANO* 371–374 (2016)
3. C. Deppisch, T. Fitzgerald, A. Raman, F. Hua, C. Zhang, P. Liu, M. Miller, JOM **58**(6), 67–74 (2006)
4. W.J. Plumbridge, J. Mater. Sci. **31**, 2501–2514 (1996)
5. T. Fałat, P. Matkowski, B. Płatek, C. Zandén, J. Felba, L.-L. Ye, J. Liu, *EMPC* (2013)
6. B. Carlberg, L. Ye, J. Liu, Mater. Lett. **75**, 229–232 (2012)
7. M. Raza, A. Westwood, A.P. Brown, C. Stirling, J. Mater. Sci. **23**, 1855–1863 (2012)
8. B. Carlberg, T. Wang, J. Liu, D. Shangguan, Microelectron. Int. **26**, 28–36 (2009)
9. R. Prasher, Proc. IEEE **94**, 1571–1586 (2006)
10. T. Jensen, R. Lasky, *Pan Pacific*, 1–9 (2020)
11. M. Plötner, B. Donat, A. Benke, Cryogenics **31**, 159–162 (1991)
12. F. George, V. Voort, *Metallography principles and practice* (ASM International, Almere, 1984), pp.136–138
13. Y.F. Lin, H. Hung, H.Y. Yu, C. Kao, Y. Wang, J. Mater. Sci. **31**, 10161–10169 (2020)
14. Y. Tian, C. Liu, D. Hutt, B. Stevens, J. Electron. Mater. **43**, 594–603 (2014)
15. C. Dasarathy, Pract. Metallogr. **7**, 44–46 (1970)
16. C. Dasarathy, Metall. Mater. Trans. B **1**, 1784–1786 (1970)
17. L.D.D. Morais, S. Chevalliez, S. Mouleres, Microelectron. Reliab. **54**(9–10), 1802–1805 (2014)
18. J.R. Michael, D. Perry, D.P. Cummings, J. Walraven, M. Jordan, Micros. Microanal. (2022). https://doi.org/10.1017/S1431927622000496
19. T. Dang, D. Shima, G. Balakrishnan, A. Chen, R. Bedford, J. Vac. Sci. Technol. B **30**(6), 060602 (2012)
20. L.D.D. Morais, S. Chevalliez, S. Mouleres, Microelectron. Reliab. **54**, 1802–1805 (2014)
21. L.-C. Huang, Y.-P. Zhang, C.-M. Chen, L.-Y. Hung, Y.-P. Wang, Mater. Charact. **184**, 111673 (2022)
22. F. Shieu, C.-C. Chen, J.G. Sheen, Z. Chang, Thin Solid Films **346**, 125–129 (1999)
23. Y.M. Liu, T. Chuang, J. Electron. Mater. **29**, 405–410 (2000)
24. K. YunAh, B. JoHyun, J. HyunHye, C. MiKyoung, K. YoungDo, R. DongSu, P. DongJoo, K. JinYong, *ECTC* (2021)
25. Y.-Y. Wu, W. P. Lin, C. C. Lee, *IEEE Int. Symp. Adv. Packag. Mater*. (2013)
26. S. Hassam, J. Rogez, Z. Bahari, J. Chem. Thermodyn. **70**, 168–175 (2014)

Publisher's Note Springer Nature remains neutral with regard to jurisdictional claims in published maps and institutional affiliations.

Springer Nature or its licensor holds exclusive rights to this article under a publishing agreement with the author(s) or other rightsholder(s); author self-archiving of the accepted manuscript version of this article is solely governed by the terms of such publishing agreement and applicable law.